eNeuro

Network mechanisms generating abnormal and normal hippocampal High
Frequency Oscillations: A computational analysis

Network mechanisms generating abnormal and normal hippocampal High Frequency Oscillations: A computational analysis

Abstract

High-frequency oscillations (HFOs) are an intriguing potential biomarker for epilepsy, typically categorized according to peak frequency as either ripples (100-250 Hz) or fast ripples (> 250 Hz). In the hippocampus, fast ripples were originally thought to be more specific to epileptic tissue, but it is still very difficult to distinguish which HFOs are caused by normal versus pathological brain activity. In this study we use a computational model of hippocampus to investigate possible network mechanisms underpinning normal ripples, pathological ripples, and fast ripples. Our results unify several prior findings regarding HFO mechanisms, and also make several new predictions regarding abnormal HFOs. We show that HFOs are generic, emergent phenomena whose characteristics reflect a wide range of connectivity and network input. Although produced by different mechanisms, both normal and abnormal HFOs generate similar ripple frequencies, underscoring that peak frequency is unable to distinguish the two. Abnormal ripples are generic phenomena that arise when input to pyramidal cells overcomes network inhibition, resulting in high-frequency, uncoordinated firing. In addition, fast ripples transiently and sporadically arise from the precise conditions that produce abnormal ripples. Lastly, we show that such abnormal conditions do not require any specific network structure to produce coherent HFOs, as even completely asynchronous activity is capable of producing abnormal ripples and fast ripples in this manner. These results provide a generic, network-based explanation for the link between pathological ripples and fast ripples, and a unifying description for the entire spectrum from normal ripples to pathological fast ripples.

Significance Statement

Roughly 0.25% of people throughout the world suffer from uncontrolled epilepsy, largely due to our incomplete understanding of how seizures are generated. This motivates the search for new epilepsy biomarkers, one of the most promising of which are high-frequency oscillations (HFOs): focal, brief field potential signals of 80 Hz or more. Not all HFOs are pathological, however, and despite 20 years of research, it is still unclear how to distinguish normal from pathological HFOs. We use a computational model to investigate the network properties capable of generating two types of HFOs, ripples and fast ripples. Our model indicates that a range of physiological conditions are capable of producing the full spectrum of HFOs, from normal ripples to "epileptic" fast ripples.

Introduction

High frequency oscillations (HFOs) have attracted much attention over the past several years as a potential biomarker of epileptic tissue. HFOs are brief oscillations (usually <100 ms) over 80 Hz that stand out from background. They were originally discovered in the CA1 region of normal hippocampus (Buzsáki, 1986; Buzsaki et al., 1992) and called "ripples" (<250 Hz). Bragin and colleagues subsequently found that HFOs were increased in epileptic hippocampus in humans (Bragin et al., 1999). They also identified a new class of faster oscillations (>250 Hz), termed "fast ripples." Since that time, much effort has focused on characterizing the role of HFOs in epilepsy (Jacobs et al., 2012).

While these studies suggest the potential of HFOs as a novel epilepsy biomarker, subsequent human studies have demonstrated the difficulty in determining whether a given HFO stems from normal or

epileptic processes (Engel et al., 2009; Kerber et al., 2014). Both ripples and fast ripples are increased in epileptic tissue (Jirsch et al., 2006; Urrestarazu et al., 2007), though the ratio between them is altered in epilepsy (Staba et al., 2007). Fast ripples are seen in normal neocortex (Coppola et al., 2005; Jones et al., 2000) and have recently been recorded in hippocampal tissue that does not participate in seizures (Kucewicz et al., 2014), thus illustrating the need to better understand the mechanisms underpinning different varieties of HFOs (Jefferys et al., 2012).

Initial studies indicated that normal and epileptic HFOs are produced by different mechanisms. Ripples are formed in normal tissue by IPSPs when interneurons fire in phase with the oscillation and pyramidal cells fire very sparsely (Ylinen et al., 1995). Subsequent computational studies have further bolstered this finding (Taxidis et al., 2012; Brunel and Wang, 2003). In contrast, large numbers of pyramidal cells become active during pathological HFOs (Bragin et al., 2011). It is currently unclear exactly how networks produce fast ripples. Proposed mechanisms include networks of axo-axonal gap junctions (Roopun et al., 2010; Traub et al., 2005), recurrent synapses between pyramidal cells (Dzhala and Staley, 2004), asynchronous input from CA3 to CA1 (Demont-Guignard et al., 2012), and reduced spike-time precision resulting in the emergence of two out-of-phase clusters (Foffani et al., 2007; Ibarz et al., 2010). While each of these hypotheses has merit, they have been difficult to test experimentally due to limitations in available recording technology. In addition, each of the above theories is subject to important constraints upon the network—in each case the fast ripples arise only under specific conditions.

In this paper we develop a computational model of hippocampus with the goal of determining which network phenomena are necessary and/or sufficient to produce normal ripples, pathological ripples, and fast ripples, as well as to explore mechanistic links between these rhythms. We use a physiologically realistic model of hippocampus (the "biophysical model") in which we vary two generic network properties: the number of inhibitory connections and the strength of excitatory input to all cells. This model allowed exploration of generic network effects on HFOs. However, given the remarkable capacity for distinct mechanisms to generate similar HFOs, we also explored how HFOs may arise generally, independent of any specific network structure. In essence, an HFO is produced by the summation of IPSPs or APs recorded at the electrode. Therefore, we also develop a constructed local field potential ("constructed LFP") model that explicitly controls when IPSP and AP waveforms occur, without any network structure. This constructed LFP model enables exploration of generic network properties necessary to generate HFOs, such as synchronous versus asynchronous firing.

We show that HFOs are an emergent phenomenon produced over a broad range of connectivity structures and levels of synaptic input. While similar results have been demonstrated in models of normal HFOs, our model produces the full spectrum from gamma frequencies to fast ripples, and uncovers several novel characteristics of epileptic HFOs. First, the model predicts that HFOs in the ripple range can be produced by either epileptic (i.e. APs (Bragin et al., 2011)) or normal (i.e. IPSPs (Ylinen et al., 1995)) mechanisms, and that peak frequency is unable to distinguish between the two. Second, we show that fast ripples are generic phenomena that are generated by APs and arise when synaptic input overcomes network inhibition enough to allow out of phase firing. Third, ripples produced by APs are prone to transient shifts into fast ripples, which may explain why fast ripples are often inconsistent in experimental recordings. Finally, we show that HFOs are a generic property of active neural populations and can be generated without any specific network structure, even with completely asynchronous activity.

Models

Biophysical Model

Our biophysical model of hippocampus was simulated using NEURON 7.3 (Hines and Carnevale, 1997) and is based upon two previously published models of hippocampal oscillations. The first described the interplay between gamma and theta oscillations in normal hippocampus due to feedback inhibition from basket and OLM cells (Tort et al., 2007). The second adapted the same network structure to demonstrate how ripples (< 250 Hz) arise when epileptic pathologies are present in the network, based upon the relationship between inhibitory interneurons, network connectivity, and synaptic drive to the pyramidal cells (Stacey, Lazarewicz, and Litt, 2009). This latter study did not include the OLM cells since they only affected the much slower theta (< 10 Hz) frequencies in the first model.

Both of those models used blocks of 80 pyramidal cells with 20 basket cells, and the output generated from the membrane voltages of each cell. In the current model, all cellular and synaptic parameters are identical to the previous work (Tort et al., 2007; Stacey, Lazarewicz, and Litt, 2009). Each pyramidal cell has five compartments (basal dendrite, soma, and three-compartment apical dendrite) and the basket cells have a three-compartment soma. We made two alterations to the model. All cells are given 3-dimensional coordinates as a two-layer planar disk placed 50 microns from a recording electrode (see below), and the number of pyramidal cells is increased to 3080.

The pyramidal cells were conceptually divided into 80 "active" cells and 3000 "satellite" cells. As shown in Fig. 1, each of the active pyramidal cells has efferent AMPAergic synapses with 2 or 3 basket cells, and receives GABAergic synapses from all 20 basket cells. The satellite pyramidal cells' only connections are the GABA synapses from basket cells; they represent the large number of neighboring pyramidal cells *in vivo* that receive divergent inhibitory connections from interneurons. Since they receive no input other than IPSPs, effectively their sole purpose in the simulation is to magnify the IPSP current that is recorded at the LFP electrode. Basket cells send efferent GABAergic synapses to all 3080 pyramidal cells, receive AMPAergic synapses from 10 active pyramidal cells, and are coupled to each other with somatic gap junctions, as seen experimentally wherein they form a synchronous syncytium (Amitai et al., 2002; Stacey, Lazarewicz, and Litt, 2009). Thus, the basic connectivity of this model consists only of the inhibitory feedback between pyramidal and basket cells. This reduced structure assures the model is restricted to phenomena present within this generic connectivity.

The only driving input to the model simulates the primary excitation present *in vivo*: afferent synaptic activity. From the point of view of each cell, these inputs arriving from different brain regions can be modeled as random synaptic events, or "synaptic noise." Synaptic noise was previously shown to be capable of producing high frequency oscillations (Stacey, Lazarewicz, and Litt, 2009), and was recently shown to provoke seizures *in vitro* (Jirsa et al., 2014). Thus, the afferent activity on both basket and pyramidal cells was modulated by varying the intensity of AMPA "noise" synapses. Satellite pyramidal cells did not receive such noise synapses; their only input was IPSPs from basket cells. For each noise synapse, the time between subsequent synaptic events followed an exponential distribution, so that the arrival of synaptic noise events was a Poisson process, independent from cell to cell. The mean of this distribution determined the overall noise intensity, with smaller mean inter-event interval implying greater intensity. For low intensities it has already been shown that the model generates gamma oscillations (Tort et al., 2007), typical of the PING phenomenon (Traub, Jefferys, and Whittington, 1997). In this work, we describe how the peak frequency of the network LFP output increases accordingly as synaptic drive increases, so that the model produces the full spectrum of fast oscillations: gamma, fast gamma, ripples, and fast ripples.

This model enabled the simulation of sharp wave ripples by increasing the intensity of synaptic noise received by either active pyramidal cells or basket cells, in a manner similar to the mean-field model of Demont-Guignard et al. (2012). Simulated sharp waves lasted for 35 ms in our model, with onset and offset following a Gaussian distribution ($\sigma = 7$ ms) across the neuronal population (to reproduce the physiological appearance of sharp waves and avoid nonphysiological, hypersynchronous onset).

The LFP recorded from neural activity was simulated by determining the voltage seen by the electrode from every compartment of every cell. This was done by recording the transmembrane current in all N compartments (Malmivuo and Plonsey, 1995) and calculating

$$V(\vec{r}_e, t) = \frac{\rho}{4\pi} \sum_{j=1}^{N} \frac{I_j(t)}{|\vec{r}_e - \vec{r}_j|}, \tag{1}$$

where $V(\vec{r}_e, t)$ is the net electric potential at the recording electrode at time t, ρ is the extracellular resistivity, I_j is the transmembrane current in compartment j, and $|\vec{r}_e - \vec{r}_j|$ is the distance between compartment j and the recording electrode (these distances ranged from 50 to 215 microns). The quantity ρ was set to 351 $\Omega \cdot$ cm (Latikka, Kuurne, and Eskola, 2001), and all neurons were located in a plane whose closest point was 50 microns from the simulated recording electrode (see Fig. 1B for a schematic of the spatial arrangement of the network and recording electrode). NEURON code for the model is available in ModelDB (Hines et al., 2004).

Constructed LFP Model

One major goal of this work is to determine the generic mechanisms that produce epileptic and normal HFOs. We sought to answer, independent of any network structure, what type of activity is *necessary and sufficient* to produce each type of HFO. As it is impossible to simulate all potential network configurations, we developed a more basic method of producing neural signals. We explicitly defined the onset times for a large number of either IPSP or AP waveforms (results shown in Figs. 8, 9, and 10). This model did not include any neuronal structure; it was simply a mathematical reconstruction of a number of IPSP or AP waveforms, using the same waveforms generated by the biophysical model. The goal of this model was to show, under completely controlled conditions, how the LFP would appear if it were generated purely by either type of waveform. The model allowed an explicit demonstration of the differences between these two cases, and also enabled exploration of the relationship between variability in cell firing and network output. To generate this output, we recorded from 200 microns away the LFP voltage produced by an AP in a single pyramidal cell in our biophysical model, as well as that produced by a basket cell IPSP onto a pyramidal cell. These two waveforms, which we denote $h_{AP}(t)$ and $h_{PSP}(t)$, were used as templates for the output of each AP or IPSP. We then simulated a population of cells producing these waveforms at specific times using the process described below.

Two different statistical procedures (described shortly) were used to generate a sequence of event times (modeled as Dirac delta functions) for each of N neurons, with each event representing the trigger time of either an AP or IPSP:

$$s_i(t) = \sum_{j=1}^{n_i} \delta(t - t_i^j), \tag{2}$$

where $s_i(t)$ is the event sequence of the ith neuron, n_i is the total number of events of the ith neuron, and t_i^j is the time of the jth event for the ith neuron. The contribution to the net LFP by the ith neuron,

$V_i(t)$, is then the convolution of s_i with either an AP or PSP waveform, $h_{AP/PSP}(t)$:

$$V_i(t) = \int_{-\infty}^{\infty} s_i(\tau) h_{AP/PSP}(t - \tau) d\tau. \tag{3}$$

The net recorded LFP, $V_N(t)$, is simply the sum of the contributions from all neurons:

$$V_N(t) = \sum_{i=1}^{N} V_i(t). \tag{4}$$

Note that this simple model does not consider the effect of neuron location or complex electrode filtering on the recorded LFP waveform.

Synchronous Constructed LFP Model

We used the constructed model to determine the output of a network that is driven by a defined periodic input. This simulates a situation in which there is some physiological process driving all cells nearly synchronously at a certain frequency. This is similar to the pyramidal-interneuron gamma feedback loop in our biophysical model and others (Traub, Jefferys, and Whittington, 1997), but there are many physiological situations similar to this (e.g. theta rhythm, thalamocortical loops, etc). In effect, a large number of cells receive a similar input that influences their firing, similar to having a "master clock" in the system with some random variation in each cell's firing. We use these conditions to compare the ability of synchronous APs versus synchronous PSPs to generate HFOs. The input was set to a specific frequency, and each cell responded to that input with some "jitter" to represent intercellular variability. The jitter was Gaussian distributed for each cell, as defined by the standard deviation σ_{jitter}. The time of the jth event of neuron i was therefore given by

$$t_i^j = jT + \mathcal{N}(0, \sigma_{\text{jitter}}^2), \tag{5}$$

where T determines the period of network oscillation. Population events remain periodic indefinitely, and the parameter σ_{jitter} determines the degree of event synchrony, with smaller values of σ_{jitter} implying greater synchrony (see Fig. 9A for a depiction of the effect of this parameter).

Asynchronous Constructed LFP Model

However, under physiological conditions there is not always a "master clock" driving the network at a given frequency. One might expect that, in the absence of any communication between cells, the population output would be purely random. However, several results from our biophysical model suggested that even uncoupled networks sometimes produce coherent oscillations when the pyramidal cells are firing at similar frequencies. To explore this unexpected result, we created another implementation of this LFP model to generate asynchronous network events. The goal of this model was to explore the emergence of HFOs from asynchronously-spiking cells.

The underlying statistical procedure for generating event sequences assumed that a) the entire population of neurons had a mean event rate, but that there was variability in each cell's specific rate (as well as in each cell's initial phase), and b) each cell also exhibited variability, or "jitter," from event to event. These sources of variability, as well as the independence of all event sequences, were important to investigating the possibility that asynchronous neuronal spiking might generate ripples and fast ripples. Formally, inter-event jitter was modeled by assuming that given the jth event of neuron i occurs at time t_i^j, the

next event t_i^{j+1} will occur at some later time Gaussian-distributed about neuron i's intrinsic inter-event interval, μ_i:

$$p(t_i^{j+1} = t | \text{last event time} = t_i^j) = \mathcal{N}(t_i^j + \mu_i, \sigma_{\text{jitter}}^2). \tag{6}$$

To account for population heterogeneity in intrinsic frequency, each μ_i was drawn from $\mathcal{N}(\mu_{\text{pop}}, \sigma_\mu^2)$. The parameter σ_μ therefore quantifies how similar the intrinsic firing rates are among *different cells*, whereas σ_{jitter} quantifies how consistent an *individual cell's* firing rate is. Note that without the presence of any form of coupling between the different "neurons" (i.e. event sequences) in the population, all neurons undergo events independently, resulting in completely asynchronous network dynamics. (Neuronal events were initialized with uniformly random values, so that the network began in an asynchronous state.) We studied the generation of ripples and fast ripples in this model while fixing the population mean μ_{pop} to be 5 ms (corresponding to a mean population frequency of 200 Hz). Simulations using AP waveforms featured 100 different cells, while those using IPSP waveforms featured 1500 different cells (reflecting the much larger number of synapses—in comparison with spiking compartments—which contribute to the LFP).

Analytic proof of HFOs from asynchronous firing

In this section we present an analytic solution proving that HFOs can arise from purely asynchronous firing. Consider a signal $g(t)$ generated by convolving a waveform (such as an AP or IPSP waveform) with a periodic train of delta functions that occur with frequency f_0. The Fourier transform of this signal, $G(f)$, will feature peaks at f_0 and its harmonics and will have an amplitude of zero at all other frequencies. Then consider the signal generated by summing N randomly-shifted copies of $g(t)$,

$$g_N(t) = \sum_{j=1}^{N} g(t - \tau_j), \tag{7}$$

where τ_i are independent and identically-distributed random variables, each with probability density function $p(\tau_i) = \text{unif}(0, \frac{1}{f_0})$. The function $g_N(t)$ crudely represents the LFP generated by a population of independent neurons all firing at the same frequency but with random phase. Somewhat counterintuitively, the expected amplitude of this signal does not go to zero as N increases, but rather increases with N. This can be seen by first considering the Fourier transform of the summed signal, $G_N(f) = \left[\sum_{j=1}^{N} e^{i\theta_j} \right] G(f)$, where $\theta_j = -2\pi f \tau_j$.

The expected squared-amplitude at a given frequency, $E\left\{ |G_N(f)|^2 \right\}$, can be determined by defining the random variable $A = \sum_{j=1}^{N} e^{i\theta_j}$ and first computing its expected squared amplitude:

$$
\begin{aligned}
E\left\{ |A(f)|^2 \right\} &= \int_0^{1/f_0} d\tau_1 d\tau_2 \ldots d\tau_N \ p(\tau_1)\, p(\tau_2)\ \ldots\ p(\tau_N)\ |A(f)|^2 \\
&= f_0^N \int_0^{1/f_0} d\tau_1 d\tau_2 \ldots d\tau_N\ |A(f)|^2
\end{aligned}
\tag{8}
$$

Making the change of variables $d\tau_i = -d\theta_i/2\pi f$ gives:

$$
\begin{aligned}
&= \left(\frac{-f_0}{2\pi f}\right)^N \int_0^{2\pi f/f_0} d\theta_1 d\theta_2 \dots d\theta_N \ |A(f)|^2 \\[2mm]
&= \left(\frac{-f_0}{2\pi f}\right)^N \int_0^{2\pi f/f_0} d\theta_1 d\theta_2 \dots d\theta_N \left(\sum_{j=1}^N e^{i\theta_j}\right)\left(\sum_{k=1}^N e^{-i\theta_k}\right) \\[2mm]
&= \left(\frac{-f_0}{2\pi f}\right)^N \sum_{j=1}^N \sum_{k=1}^N \int_0^{2\pi f/f_0} d\theta_1 d\theta_2 \dots d\theta_N \ e^{i(\theta_j - \theta_k)} \\[2mm]
&= \left(\frac{f_0}{2\pi f}\right)^2 \sum_{j=1}^N \sum_{k=1}^N \int_0^{2\pi f/f_0} d\theta_j d\theta_k \ e^{i(\theta_j - \theta_k)} \\[2mm]
&= \left(\frac{f_0}{2\pi f}\right)^2 \left[\left(\frac{2\pi f}{f_0}\right)^2 N + 4\sin^2\left(\frac{2\pi f}{f_0}\right) N(N-1)\right] \\[2mm]
&= N + 4N(N-1)\left(\frac{f_0}{2\pi f}\right)^2 \sin^2\left(\frac{2\pi f}{f_0}\right) \qquad (9)
\end{aligned}
$$

Combining this result with the fact that $G_N(f) = 0$ for all non-harmonic frequencies, we have

$$
E\left\{|G_N(f)|^2\right\} = \begin{cases} N|G(f)|^2, & \text{if } f = nf_0 \ (n = 1, 2, 3...) \\ 0, & \text{otherwise} \end{cases} \qquad (10)
$$

Thus, the expected value in the frequency domain is to have a peak at f_0 and its harmonics, scaled by N. In other words, the LFP of a population of N asynchronously spiking (but perfectly frequency-locked) neurons will feature a coherent oscillation at that same frequency, whose squared-amplitude scales as N. (A perfectly *synchronous* and frequency-locked population of neurons, on the other hand, will feature a coherent LFP oscillation whose squared-amplitude scales as N^2.) Note that there is a special case for the asynchronous population: with a very large number of individual waveforms in which the phases are *perfectly spaced*, $g_N(t)$ will be flat, but this result is unlikely to occur for any particular realization of the random variables θ_j, or realistic distribution of real cells.

This derivation therefore proves that a network of asynchronous cells, if firing at the same rate, is likely to produce a coherent oscillation. In a more heterogeneous network, this affect would be attenuated when firing rates were dissimilar and augmented when they were similar. Of note, since the output voltage is additive, any transient instance in which a subset of cells reached these conditions would likely produce a brief oscillation of those cells superimposed upon a more random background of uninvolved cells.

Data Processing

All spectrograms were obtained using a sliding Gaussian window with a standard deviation of 10 ms and a frequency resolution of 4 Hz. Fast ripples were defined to occur when the peak normalized power in the fast ripple band (> 250 Hz) exceeded the peak normalized power in the ripple band (100–250 Hz).

The normalized power values depicted in Figs. 9 and 10 were computed by first applying Thomson's multitaper power spectral density estimate (Thomson, 1982) to a given waveform, then determining the total power contained within 5 Hz of the nominal frequency f. Each square represents an average over 100 different realizations of the "synchronous constructed LFP model" described above.

Results

HFOs generated by input to either basket cells or pyramidal cells

We first used the biophysical model to determine the parameters necessary to produce the full range of HFOs. We found that HFOs were elicited through two distinct mechanisms: coherent firing of the 20 basket cells (which sent GABAergic connections to all 3080 pyramidal cells) or the 80 active pyramidal cells (see Fig. 1). In both cases, coherent firing arose when the noisy synaptic input reached high enough levels to cause the majority of each cell type to fire. Fig. 2 shows the results of elevated input to the basket cell population. Power spectral density (PSD) plots from the LFP were generally unimodal, and peak network frequency increased monotonically with increasing intensity of noisy synaptic input, spanning a range from gamma oscillations to fast ripples (Fig. 2A). Peak network frequency (Fig. 2A) closely matched mean basket cell firing rate (Fig. 2B), indicating that the LFP resulted from IPSPs induced in pyramidal cells due to basket cell firing. Basket cell action potential waveforms were present but contributed very little to the LFP, due to basket cells' small size. Although the peak frequency did reach the fast ripple range, it is crucial to point out that the amplitude of network oscillations decreased substantially as peak network frequency increased (Fig. 2C). The total power was much higher in gamma (< 100 Hz) frequencies, and reached very small levels beyond 200 Hz (Fig. 2C). Such small-amplitude oscillations would be unlikely to resolve above background noise levels in a live recording.

Network activity was distinctly different when noisy input was delivered to pyramidal cells rather than basket cells (Fig. 3A). The spectral content was bimodal due to different firing rates of the basket and the active pyramidal cells. The higher frequency was due to basket cell firing (Fig. 3B), which dominated the output for most low noise intensities. However, in contrast to the prior case (Fig. 2), at higher frequencies the lower frequency peak, produced by pyramidal cell action potentials, dominated. This signal became very prominent, as evidenced by the persistence of high signal power (3C). In other words, when the pyramidal cells are driven by varying levels of synaptic activity, they produce a range of strong oscillations from 60-150 Hz which are dominated by IPSPs at low frequency and APs at high frequency. The synaptic input in the latter case reaches very high levels, producing very fast pyramidal cell firing that would only be expected in highly active conditions such as epilepsy (see Discussion). Thus, this model shows the transition from what are likely normal to epileptic HFOs. However, with this configuration (all connections intact) it was impossible to elicit fast ripples for two reasons: 1) the basket cell inhibition effectively limited the peak frequency of pyramidal cell firing; and 2) pyramidal cells were synchronized when inhibitory feedback was intact.

Peak frequency insufficient to disambiguate ripple mechanisms

HFOs have traditionally been categorized based upon peak frequency into fast gamma, ripples, and fast ripples. However, as shown in Figs. 2 and 3, our biophysical model was capable of generating ripples through both normal and epileptic conditions, similar to recent experimental work (Aivar et al., 2014). This leads to the question of whether ripples produced by these disparate mechanisms can be distinguished. To demonstrate the similarities, we depict example waveforms, spectrograms, and raster plots for simulated sharp-wave ripples elicited by these two different mechanisms (Fig. 4). In panels (A-D) we show examples of approximately 200 Hz rhythms elicited by elevated basket cell activation (noise intensity = 0.25×10^{-4} nA^2). These LFP rhythms reflect synchronous IPSPs induced in pyramidal cells, consistent with previous experimental studies (Buzsaki et al., 1992; Ylinen et al., 1995). The sparse firing of pyramidal cells in these examples contrasts sharply with the alternative scenario (Figs. 4(E-H)) in which active pyramidal cells, rather than basket cells, were directly activated (noise intensity = 0.77 nA^2).

Figs. 4(E-H) show that the peak frequency was again around 200 Hz, but network activity was dramatically different: the elevated activity of pyramidal cells induced increased basket cell firing, so that pyramidal cell spiking and basket cell-induced IPSPs contributed fairly equally to the LFP oscillations. More importantly, there was more high frequency activity with AP-generated ripples (see increased 300-400 Hz power in spectrograms E-H), while the IPSP signals (A-D) were smoother without high frequency content. These examples illustrate the importance of evaluating more than simply the peak frequency when attempting to discern the underlying cause or pathogenicity of HFOs.

Effects of compromised inhibition

The model was unable to elicit fast ripples with any level of input when network inhibition was intact (Fig. 3). We therefore investigated the effects of compromising network inhibition on fast ripple generation. We randomly disabled a specified percentage of basket-to-pyramidal cell GABAergic connections, then generated 50 consecutive sharp waves by transiently increasing the random synaptic input to active pyramidal cells. This allowed determination of the proportion of sharp waves that included fast ripple events. (The peak frequency in the fast ripple band had to have higher spectral power than the peak frequency in the ripple band for at least 25% of the duration of the sharp wave in order to count as a fast ripple event.) From the results shown in Fig. 5, disruption of inhibitory connections had a profound impact on the emergence of fast ripples: as basket cell connections were lost, the same input that had previously generated only sharp wave-ripple events began to produce fast ripples as well.

Loss of network inhibition has two important consequences in our model. First, fewer inhibitory connections imply a relatively greater contribution to the LFP from pyramidal cell APs compared to IPSPs. Second, loss of feedback inhibition erodes the ability of the network to synchronize, until at extreme levels the network is completely uncoupled, leading to asynchronous pyramidal cell spiking. Yet, as shown in Fig. 5B, even asynchronous networks generated coherent ripple and fast ripple rhythms. These observations raise two questions: 1) how does asynchronous neuronal spiking generate ripples and fast ripples, and 2) to what degree are AP-dominated versus PSP-dominated LFPs capable of producing fast ripples?

Generation of ripples and fast ripples from asynchronous network activity

To address the first question, we ran simulations in which uncorrelated noisy input was delivered to the 80 active pyramidal cells, with no other cells in the network and no coupling between pyramidal cells. Fig. 6A shows that this completely asynchronous network generated coherent network oscillations characterized by a pronounced fundamental frequency and a lower-power first harmonic. This is somewhat similar to the bimodal PSDs observed when pyramidal cells received input when feedback inhibition was intact (Fig. 3A), except that the frequencies are higher and—importantly—there were no individual cells that fired at the frequency of the second harmonic (Fig. 6B). Note that the second harmonic constitutes a fast ripple frequency, and that unlike the situation in which basket cells were directly activated (Fig. 2C), in this case the oscillation amplitude does not appreciably diminish with increasing noise intensity. Instead, total power remained roughly constant as noise intensity increased (Fig. 6C), until all pyramidal cells went into depolarization block (the raster plot in Fig. 6B shows evidence of several cells already in depolarization block at the highest noise intensity which still sustained network oscillations).

Fig. 6A shows that the ripple (<250 Hz) frequencies dominated despite the presence of the fast ripple harmonics. However, our observations of the instantaneous signals revealed that there were many instances in which fast ripples dominated, just as in Fig. 5 B,C. In order to investigate how such fast ripple activity emerges in this asynchronous network, we ran a long simulation (20,000 ms) (Fig. 7) using the same uncoupled pyramidal cell network as used in Fig. 6, with the noise intensity set to the highest

level that still sustained network oscillations (0.77 nA^2). At this level of noise intensity, some neurons went into depolarization block (Fig. 6B), while the remaining firing neurons all had similar firing rates due to their similar dynamics. As shown in Fig. 7A, we observed that strong ripple oscillations at ~ 200 Hz (which matched the mean firing rate of neurons not in depolarization block) dominated the LFP the majority of the time, but that fast ripple episodes emerged spontaneously, typically lasting 20-50 ms. Spike-time histograms relative to ripple phase indicated that the ripple episodes had a single cluster (Fig. 7B), while fast ripple episodes occurred due to two out-of-phase spiking clusters (Fig. 7C). This is similar to what has been proposed previously by Menendez de la Prida's group (Foffani et al., 2007; Ibarz et al., 2010). Most striking, however, is that in our results there is no organizing mechanism for such bi-cluster dynamical states–they emerge briefly and spontaneously from asynchronous activity in a completely uncoupled network. Such fast ripples are therefore not a result of decreased spike timing reliability, but emerge by chance when the randomly-evolving spike-time structure happens to assume a bimodal form.

While it may seem counterintuitive that an uncoupled network could produce a coherent oscillation, this idea has been investigated previously (Ray et al., 2008; Nunez, 1995), and in the Methods section we provide an analytical derivation proving that coherent LFP oscillations will emerge from a population of frequency-locked, asynchronously firing neurons (Eqns. 7-10). The results shown in Figs. 6 and 7 extend the results of that derivation by demonstrating that coherent oscillations will emerge even when there is some heterogeneity in mean firing rate from cell to cell.

However, given the complexity of the biophysical model, it is possible that the coherence was due to some artifact of the simulation itself. We therefore developed a more basic method to explore this phenomenon, devoid of any network structure. We implemented a simplified model stripped of all biophysical details, in which LFP signals were "constructed" by convolving action potential waveforms with a number of randomly-generated spike trains, each representing the firing times of a single cell. This model assumed the existence of a network drive for cells to fire *near* a given frequency, but with two primary sources of variability in the spiking of each cell. This model is agnostic to the mechanisms that produced a given activity, and instead simply shows how the LFP would appear if such activity occurred. *From this point on, all results are from this constructed LFP model, rather than the biophysical model.*

The constructed LFP model assumed that there were many cells firing *near* a given frequency due to conditions in the network. Although each cell was driven in similar fashion, there are two primary sources of variability in spike times that must be accounted for. The first was motivated by the fact that in the brain, each cell generally has different parameters and inputs, and thus each will have slightly different mean firing rates for a given brain state. We modeled each cell's mean inter-spike interval (ISI) μ_i as being drawn from a normal distribution with standard deviation σ_μ. The second source of variability modeled "jitter" in ISI times, since each cells' ISI typically fluctuates from spike to spike due to noise in the network, even when the mean firing rate is relatively constant over time. The degree of ISI jitter was determined by the parameter σ_{jitter}. The difference in the effects of these two parameters is depicted in Fig. 8A. (See "Asynchronous Constructed LFP Model" in Methods for further details.)

Figures 8B-E demonstrate that in a generic model of network activity stripped of all biophysical details, asynchronous neuronal activity can produce strong LFP oscillations. As in the results of the biophysical model shown in Fig. 6A, the network displayed a prominent oscillation at the overall mean cellular firing frequency (200 Hz, corresponding to $\mu = 5$ Hz), intermixed with transient fast ripple episodes. As heterogeneity in mean ISI or ISI jitter increased, the LFP became noisier, LFP oscillations less coherent, and fast ripple episodes less frequent. Fig. 8F shows the fast ripple occurrence ratio as a function of

both sources of dynamical heterogeneity, which had very similar overall effect. In both cases, fast ripple occurrence decreased as heterogeneity increased, with heterogeneity of $\sim$10% of mean ISI effectively eliminating fast ripple episodes.

Generation of fast ripples by APs versus PSPs

We observed two different mechanisms for generating fast ripples in our biophysical model: 1) direct activation of basket cells by noisy input, which was capable of eliciting coherent fast ripple rhythms, though the amplitude of such rhythms was dramatically smaller than for lower-frequency rhythms (Fig. 2); and 2) activation of pyramidal cells in networks with impaired inhibition, which saw fast ripples emerge sporadically from a baseline ripple rhythm (Fig. 7). In the former mechanism the LFP was completely dominated by IPSPs, which were powerful enough to completely suppress pyramidal cells. The latter mechanism was dominated by active currents generated by pyramidal cell action potentials. Experimentally, both IPSPs (Spampanato and Mody, 2007; Ylinen et al., 1995; Klausberger et al., 2003b; Schevon et al., 2009) and APs (Grenier, Timofeev, and Steriade, 2003; Bragin et al., 2011) have been shown to contribute to HFOs, though their respective abilities to form fast ripples has not been definitively established. To determine the capacity of each type of waveform to generate fast ripples, we constructed the LFP with explicit event times as in the previous section, but with coupling between the cells to provide synchrony. In this case, the model compared the output signals produced by either APs or IPSPs. The only parameters in this model were the nominal firing frequency and the jitter in interspike intervals, σ_{jitter} (see "Synchronous Constructed LFP Model" in Methods).

As shown in Fig. 9D–O, both AP-dominated and PSP-dominated LFPs exhibited coherent oscillations whose dominant frequency matched the nominal network burst frequency (though AP-dominated LFPs grew less "clean" as coherence decreased, as shown in Figs. 9D,G). We explored the ability of both classes of waveforms to generate fast ripples by observing how LFP oscillation amplitude was affected by increased frequency of network bursts. The color plots in Figs. 9B,C show that AP-dominated and PSP-dominated LFPs exhibited very different trends: the amplitude of AP-dominated LFPs remained constant as frequency increased, whereas the amplitude of PSP-dominated LFPs decreased dramatically with increasing frequency. These trends are even more starkly depicted in the plots of LFP waveforms shown in Fig. 9D–O. Furthermore, decoherence of network bursts (resulting from increased σ_{jitter}) had essentially the same impact upon AP-dominated LFP amplitude across all frequencies (Fig. 9B). The impact of decoherence upon PSP-dominated LFPs, on the other hand, grew more severe as frequency increased (Fig. 9C).

These results show that, independent of the underlying network structure, the actual waveforms that arise when a population of cells produces either APs or IPSPs have extremely different capacities to produce fast ripples. The short duration of APs allows a wide range of frequencies that are resistant to significant jitter among the cells. In contrast, although PSPs are theoretically able to generate fast ripple signals, the amplitude is extremely low and even small amounts of jitter abolish the signal. We conclude that, under physiological conditions, it is likely that all fast ripples are generated purely by APs, regardless of underlying network structure.

Effect of synaptic parameters on fast ripple generation by PSPs

Previous work has shown that network rhythms are dramatically affected by changes in synaptic parameters, with faster time constants (such as synaptic rise time) having a much greater impact than slower time constants (such as synaptic decay time) (Brunel and Wang, 2003). We investigated the effects of varying these synaptic parameters in our constructed LFP model, with the results shown in Fig. 10.

For all modifications (increasing and decreasing τ_{rise} and τ_{decay}), the amplitude of PSP-dominated LFPs decreased with increasing frequency, as with the standard synaptic parameters. Modifying τ_{decay} had very little effect on network rhythms (compare Figs. 10A,B with Fig. 9C), whereas decreasing τ_{rise} did result in more robust network rhythms at high frequency (Fig. 10C). With supraphysiologically fast rise time (0.5 ms), the output approached the results of APs (Fig. 9B), but was still less robust at higher frequencies. Both of these results are consistent with the findings of (Brunel and Wang, 2003). It should be emphasized, however, that in all cases increasing frequency resulted in greater sensitivity to decoherence (i.e., increased relative jitter), an effect that was not observed in AP-dominated LFPs (Fig. 9B). These results show that LFPs are unlikely to produce fast ripples even with different synaptic parameters due to their slower dynamics.

In this simplified model, therefore, PSP-dominated LFPs were in principle capable of producing fast ripples, but these rhythms were much less robust than the fast ripples generated by APs. They required extreme network coherence and produced very small amplitude signals, and would therefore be unlikely to be observed in networks with physiological levels of noise.

Discussion

Choice of models and parameters

This work has utilized two models, a biophysical model to show how network interactions produce different HFOs, and a constructed LFP model to show the differences between HFOs produced by IPSPs and APs. The biophysical model contains a simple hippocampal network, which assures that we are simulating generic, rather than structure-specific, phenomena. Because it was designed to simulate fast oscillations, it did not include the slower effects of OLM cells that produced theta oscillations in the original presentation of this model (Tort et al., 2007). Omission of OLM cells, and several other potential interneurons, does eliminate some effects that might be important in generation of particular HFOs. For instance, recent work has suggested OLM cells are involved in some HFOs (Pangalos et al., 2013; Varga, Golshani, and Soltesz, 2012), although other work showed that OLM cells were silent during HFOs (Klausberger et al., 2003a). More complex HFO models show the effects of several other interneurons in producing "normal ripples (Schomburg et al., 2012), or complex networks of axoaxonic gap junctions producing fast ripples (Simon et al., 2014). These models, and the others we have previously discussed, contain some effects not present in our model, which are likely to produce subtle differences in the HFO characteristics; however, these are not generic mechanisms of HFO generation and it is difficult to compare the results between such models. Our goal with the current model was to investigate the unifying mechanisms of HFOs, from gamma to fast ripples, which might reconcile such different networks.

One critical parameter in our biophysical model is the synaptic noise. The synaptic noise represents the physiological drive that causes cells to become excitable. The lower levels of noise intensity are easily justified, but several of the effects in this work arise only when the noise reaches extremely high levels. Such high afferent drive caused each of the cells to fire at very similar rates, at times high enough that cells began to go into depolarization block (Fig. 6A,B). While such a high level of noise intensity may seem extreme, it is actually common during epileptic conditions (Jirsa et al., 2014; Stacey, Lazarewicz, and Litt, 2009; Grenier, Timofeev, and Steriade, 2003; Dzhala and Staley, 2004; Karlócai et al., 2014) and not unlike other physiological conditions such as the Up state (Destexhe, Rudolph, and Paré, 2003). Because neighboring pyramidal cells have similar structural and dynamic parameters, their absolute refractory period and peak firing rate are also similar. Thus, when there is a strong enough network drive, cells will have similar firing rates, which we demonstrate can produce coherent oscillations regardless of network

connectivity. A recent study by Alvarado-Rojas et al. (2014) provides strong experimental support for this scenario.

We developed the constructed LFP model to answer several questions regarding how HFOs can be formed by APs versus IPSPs. This model gave us explicit control of when the events occurred, allowing us to investigate how the LFP would appear under a vast range of different network firing, independent of the specific mechanism that would produce such firing. However, it is important to point out that each waveform template (i.e. the signal produced when an AP or IPSP occurred) was actually recorded from the biophysical model. Thus, although there was no neuronal network in this model, its output is identical to any implementation of the biophysical network that produced the same firing times.

Mechanisms of normal and pathological HFOs

It is currently thought that normal ripples are produced either nearly exclusively by IPSPs (Ylinen et al., 1995; Le Van Quyen et al., 2008) or a roughly equal mixture of IPSPs and active currents (Schomburg et al., 2012), while epileptic HFOs are most likely produced predominantly by the active currents associated with population spikes (Bragin et al., 2011). Our biophysical model is consistent with this view, since noisy synaptic bombardment of either pyramidal cells or basket cells tended to produce ripples when inhibition was intact (Fig. 4). In our model this implied either a completely PSP-dominated LFP (when basket cells were activated) or an LFP comprised of roughly equal parts PSPs and active currents (when pyramidal cells were activated). As inhibition was progressively compromised, however, noisy synaptic activation began to activate pyramidal cells more strongly. This produced not only abnormal ripple oscillations, but also elicited fast ripples with increasing occurrence rate (Fig. 5).

The mechanisms underlying fast ripple generation have been more challenging to explain. Previous studies on pathological HFOs (Foffani et al., 2007; Karlócai et al., 2014; Wendling et al., 2012; Demont-Guignard et al., 2012; Aivar et al., 2014) have shown that fast ripples occur when pyramidal cells become very excitable and inhibition is compromised. Many specific mechanisms have been investigated with both computational and experimental work: axo-axonal gap junctions (Traub and Bibbig, 2000; Schmitz et al., 2001; Simon et al., 2014; Roopun et al., 2010; Traub et al., 2005), recurrent synapses (Dzhala and Staley, 2004; Ibarz et al., 2010), spike time variability (Foffani et al., 2007), uncorrelated firing (Demont-Guignard et al., 2012), decreased Ca^{2+} concentration (Aivar et al., 2014), and disconnected populations (Ibarz et al., 2010). All have demonstrated some experimental evidence, and each may exist under different conditions, but reconciling these theories has been controversial.

In this study, we take an alternative approach by focusing on the general dynamical properties of network activity necessary to generate fast ripples, rather than specific lower-level mechanisms. We provide a generic framework to identify and unify the mechanisms underpinning normal ripples, pathological ripples, and fast ripples in the hippocampus. In general, normal gamma and HFOs arise when network drive induces coherent IPSP firing. As the drive increases, pathological HFOs arise when pyramidal cells become highly active, under any particular network structure. At ripple frequencies, the output can be any combination of PSP and AP waveforms. High levels of inhibitory feedback in the network are likely to limit pathological HFOs to ripple frequencies. However, as the pyramidal cells become very active, it becomes more and more likely that they will transiently desynchronize if inhibition is insufficient. Fast ripples will then naturally emerge from pathological ripples provided there are enough spikes to produce an LFP signal, since fast ripples almost certainly must be comprised of APs (Fig. 9). Fast ripples thus do not depend upon a specific network structure or connectivity, but are a general, emergent phenomenon, corroborating that each of the aforementioned mechanisms are capable of producing them. The only

requirements to produce fast ripples are that a) pyramidal cells are very active, b) the cells can become desynchronized, and c) the LFP is dominated by APs. We predict that any network conditions that produce these effects will be capable of generating fast ripples.

Features of normal and pathological HFOs

Even after nearly two decades of research, there is still no clear way to determine whether an HFO is produced by normal or abnormal mechanisms. What is clear is that peak frequency alone is insufficient to make the distinction. Below 250 Hz, HFOs can be indicative of either completely normal activity or epileptic tissue. Fast ripples originally appeared to be more specific to epilepsy in hippocampus, but recent human data have placed that in doubt as well (Kucewicz et al., 2014). And fast ripples have been well known in normal somatosensory cortex for many years (Amassian and Stewart, 2002; Blanco et al., 2011). Thus, additional methods are needed to distinguish normal from abnormal HFOs.

Our data suggest two important aspects of abnormal HFOs that may help in future research. First, the fact that fast ripples emerge from pathological ripples may explain why they are transient and coexist with ripples on the same electrode recordings. This suggests an alternative strategy of searching for similarities between such events such as harmonic frequencies or other features, rather than assuming they are different. Second, our biophysical simulation (Fig. 4) demonstrates that although peak frequency may be similar in normal and epileptic HFOs, there are more subtle features of the signal such as high frequency band power that might distinguish them.

One potential use for these results is to guide future experiments to distinguish normal from abnormal HFOs (Engel et al., 2009). Our model predicts that epileptic hippocampal tissue will have a mixture of ripples and fast ripples, both of which may be produced by the same mechanism. The key is to identify features of those signals, other than peak frequency, that are unique to the epileptic pathology. One possibility is to compare the high frequency band power ($>$250 Hz), which is higher in AP-dominated HFOs in our model. However, the rigorous solution to this question will require large amounts of human data in which vast numbers of HFOs can be analyzed. Recent work using controlled stimulation has shown that different HFOs can be distinguished using basic features (Kucewicz et al., 2014); our results can help guide future analysis of such signals to find more comprehensive differences.

"Pathological" HFOs are generic phenomena of highly activated pyramidal cells

Our biophysical and constructed LFP models show that ripples produced by APs sporadically and transiently generate fast ripples (Figs. 5 and 7), thus providing a potential link between pathological ripples and fast ripples. While several previous studies have assumed that AP-dominated ripples result from highly synchronous pyramidal cell firing (Menendez de la Prida and Trevelyan, 2011; Bragin, Engel, and Staba, 2010), our results suggest an alternative possibility: that AP-dominated ripples in fact do not require any specific structure at all: they may result from *asynchronous* firing of a population of pyramidal cells driven near their maximum firing rate. Figs. 8B-E show how in a generic model a population of independently- and randomly-firing pyramidal cells may generate a strong ripple oscillation. This result is consistent with previous theoretical studies showing that asynchronous neuronal firing can produce coherent LFP rhythms (Ray et al., 2008; Nunez, 1995), and in the Methods section we provide an analytical derivation which further supports this idea.

We thus have shown, via biophysical modeling, a constructed LFP, and an analytical derivation, that

ripples and fast ripples emerge from very active networks even without any specific coupling between cells. As Fig. 7A shows, a heterogeneous population of uncoupled pyramidal cells all firing independently at ∼ 200 Hz (which several studies have shown to be a realistic rate under epileptic conditions (Grenier, Timofeev, and Steriade, 2003; Dzhala and Staley, 2004; Karlócai et al., 2014)) will produce a 200 Hz rhythm which sporadically doubles to 400 Hz. Fig. 7C demonstrates that such frequency doubling may be explained by a familiar mechanism: the emergence of two out-of-phase clusters (Foffani et al., 2007; Ibarz et al., 2010). It must be emphasized, however, that in our model the emergence of such a bi-cluster state is inherently different from previous work: there is no network structure or coupling of any sort in Fig. 7, and thus the emergence of fast ripples is not due to an organized population losing spike-time reliability or splitting into two independent clusters, since the ripple rhythm from which fast ripples emerge is itself generated by uncoupled, asynchronously-spiking cells.

In our model, the emergence is purely from asynchronously-spiking cells, and bi-cluster states emerge when the spike-timing distribution of the heterogeneous neuronal population happens to transiently assume a bimodal form. Thus, this mechanism is a more generalized example of that proposed in Foffani et al. (2007) and Ibarz et al. (2010), which find experimental support in the work of Jiruska et al. (2010). Our results are also consistent with the findings of Demont-Guignard et al. (2012), who devised a model showing that fast ripples are elicited in CA1 due to relatively asynchronous CA3 input. It should be noted, however, that our model additionally proposes that asynchronous pyramidal cell firing provides a mechanistic link between pathological ripples and fast ripples, thereby helping to explain why fast ripples are often intermixed with ripples (Bragin et al., 1999; Worrell et al., 2008), as well as why fast ripples are so ephemeral.

These results also potentially lead to a novel approach to thinking of so-called pathological HFOs. While it is true that the conditions capable of producing asynchronous HFOs are most likely to be seen during epileptiform activity, there are normal conditions that might also produce it. AP-dominated HFOs, both ripples and fast ripples, simply require highly active pyramidal cells that are not fully synchronized. There are many potential conditions that might produce this activity, especially within the very brief time course of an HFO. Thus it is not surprising that fast ripples are seen transiently in normal cortex (Amassian and Stewart, 2002; Kucewicz et al., 2014; Blanco et al., 2011). Therefore, to use HFOs as a biomarker of epilepsy, further study will have to evaluate not only more sophisticated features of individual HFOs, but also make use of large datasets to evaluate population features such as temporal variability and network correlations that will provide more statistical rigor.

Conclusion

Collectively, our results suggest a unifying framework for characterizing the network mechanisms underpinning HFOs, from normal ripples to pathological ripples and fast ripples. Our model demonstrates that different HFOs arise when synaptic input increases, first triggering IPSPs by activating inhibitory interneurons, then activating pyramidal cells at high gamma and ripple frequencies, then producing fast ripples if inhibition is insufficient. This transition from normal to epileptic activity as noise increases is reminiscent of recent work showing how a network moves from the normal to seizure regime (Jirsa et al., 2014). We also demonstrate that loss of inhibitory interneurons is sufficient for network rhythms to transition from IPSP-dominated normal ripples to AP-dominated pathological ripples interspersed with fast ripples. Other mechansims—such as axo-axonal gap junction coupling, recurrent chemical synapses, or reduced spike-timing reliability—are not mutually exclusive, but instead comprise a multi-dimensional space of potential mechanisms for producing fast ripples. In particular, we also show that fast ripples can result from completely asynchronous firing, and thus are an inherent behavior of networks of similar pyramidal cells. Any situation that permits cells to fire at high frequency and with similar rates will

produce "pathological" HFOs.

Distinguishing normal from pathological HFOs remains a challenging problem whose solution holds great promise for people with epilepsy. In this study we have focused on the network mechanisms that differentiate the varieties of HFOs, motivating future experimental studies to obtain a more comprehensive picture of network activity. This study also provides a foundation for investigating differential LFP signatures for normal versus pathological HFOs, and guides future experimental and clinical HFO research.

References

Aivar, Paloma, Manuel Valero, Elisa Bellistri, and Liset Menendez Prida (2014). Extracellular calcium controls the expression of two different forms of ripple-like hippocampal oscillations. *The Journal of Neuroscience* 34(8): 2989–3004.

Alvarado-Rojas, Catalina, Gilles Huberfeld, Michel Baulac, Stéphane Clemenceau, Stéphane Charpier, Richard Miles, Liset Menendez Prida, and Michel Quyen (2014). Different mechanisms of ripple-like oscillations in the human epileptic subiculum. *Annals of neurology* .

Amassian, Vahe E and Mark Stewart (2002). Motor cortical and other cortical interneuronal networks that generate very high frequency waves. *Supplements to Clinical Neurophysiology* 56: 119–142.

Amitai, Yael, Jay R Gibson, Michael Beierlein, Saundra L Patrick, Alice M Ho, Barry W Connors, and David Golomb (2002). The spatial dimensions of electrically coupled networks of interneurons in the neocortex. *The Journal of Neuroscience* 22(10): 4142–4152.

Blanco, Justin a, Matt Stead, Abba Krieger, William Stacey, Douglas Maus, Eric Marsh, Jonathan Viventi, Kendall H Lee, Richard Marsh, Brian Litt, and Gregory a Worrell (2011). Data mining neocortical high-frequency oscillations in epilepsy and controls. *Brain* 134(Pt 10): 2948–59.

Bragin, a, J Engel, C L Wilson, I Fried, and G Buzsáki (1999). High-frequency oscillations in human brain. *Hippocampus* 9(2): 137–42.

Bragin, Anatol, Simone K Benassi, Farshad Kheiri, and Jerome Engel (2011). Further evidence that pathologic high-frequency oscillations are bursts of population spikes derived from recordings of identified cells in dentate gyrus. *Epilepsia* 52(1): 45–52.

Bragin, Anatol, Jr. Engel, Jerome, and Richard J. Staba (2010). High-frequency oscillations in epileptic brain. *Current Opinion in Neurology* 23(2): 151–156.

Brunel, Nicolas and Xiao-Jing Wang (2003). What determines the frequency of fast network oscillations with irregular neural discharges? i. synaptic dynamics and excitation-inhibition balance. *Journal of neurophysiology* 90(1): 415–430.

Buzsáki, György (1986). Hippocampal sharp waves: their origin and significance. *Brain Research* 398(2): 242–252.

Buzsaki, Gyorgy, Zsolt Horvath, Ronald Urioste, Jamille Hetke, and Kensall Wise (1992). High-frequency network oscillation in the hippocampus. *Science* 256(5059): 1025–1027.

Coppola, Gianluca, Michel Vandenheede, Laura Di Clemente, Anna Ambrosini, Arnaud Fumal, Victor De Pasqua, and Jean Schoenen (2005). Somatosensory evoked high-frequency oscillations reflecting thalamo-cortical activity are decreased in migraine patients between attacks. *Brain* 128(1): 98–103.

Demont-Guignard, Sophie, Pascal Benquet, Urs Gerber, Arnaud Biraben, Benoit Martin, and Fabrice Wendling (2012). Distinct hyperexcitability mechanisms underlie fast ripples and epileptic spikes. *Annals of Neurology* 71: 342–352.

Destexhe, Alain, Michael Rudolph, and Denis Paré (2003). The high-conductance state of neocortical neurons in vivo. *Nature reviews neuroscience* 4(9): 739–751.

Dzhala, Volodymyr I and Kevin J Staley (2004). Mechanisms of fast ripples in the hippocampus. *The Journal of Neuroscience* 24(40): 8896–906.

Engel, Jerome, Anatol Bragin, Richard Staba, and Istvan Mody (2009). High-frequency oscillations: what is normal and what is not? *Epilepsia* 50(4): 598–604.

Foffani, Guglielmo, Yoryani G Uzcategui, Beatriz Gal, and Liset Menendez de la Prida (2007). Reduced spike-timing reliability correlates with the emergence of fast ripples in the rat epileptic hippocampus. *Neuron* 55(6): 930–41.

Grenier, François, Igor Timofeev, and Mircea Steriade (2003). Neocortical very fast oscillations (ripples, 80–200 hz) during seizures: intracellular correlates. *Journal of Neurophysiology* 89(2): 841–852.

Hines, Michael L and Nicholas T Carnevale (1997). The neuron simulation environment. *Neural Computation* 9(6): 1179–1209.

Hines, Michael L, Thomas Morse, Michele Migliore, Nicholas T Carnevale, and Gordon M Shepherd (2004). Modeldb: a database to support computational neuroscience. *Journal of computational neuroscience* 17(1): 7–11.

Ibarz, Jose M, Guglielmo Foffani, Elena Cid, Marion Inostroza, and Liset Menendez de la Prida (2010). Emergent dynamics of fast ripples in the epileptic hippocampus. *The Journal of Neuroscience* 30(48): 16249–61.

Jacobs, J, R Staba, E Asano, H Otsubo, JY Wu, M Zijlmans, I Mohamed, P Kahane, F Dubeau, V Navarro, et al. (2012). High-frequency oscillations (hfos) in clinical epilepsy. *Progress in Neurobiology* 98(3): 302–315.

Jefferys, John G R, Liset Menendez de la Prida, Fabrice Wendling, Anatol Bragin, Massimo Avoli, Igor Timofeev, and Fernando H Lopes da Silva (2012). Mechanisms of physiological and epileptic HFO generation. *Progress in Neurobiology* 98(3): 250–64.

Jirsa, Viktor K, William C Stacey, Pascale P Quilichini, Anton I Ivanov, and Christophe Bernard (2014). On the nature of seizure dynamics. *Brain* 137(8): 2210–2230.

Jirsch, JD, E Urrestarazu, P LeVan, A Olivier, F Dubeau, and J Gotman (2006). High-frequency oscillations during human focal seizures. *Brain* 129(6): 1593–1608.

Jiruska, Premysl, Gerald T Finnerty, Andrew D Powell, Noosheen Lofti, Roman Cmejla, and John GR Jefferys (2010). Epileptic high-frequency network activity in a model of non-lesional temporal lobe epilepsy. *Brain* 133(5): 1380–1390.

Jones, Michael S, Kurt D MacDonald, ByungJu Choi, F Edward Dudek, and Daniel S Barth (2000). Intracellular correlates of fast (> 200 hz) electrical oscillations in rat somatosensory cortex. *Journal of Neurophysiology* 84(3): 1505–1518.

Karlócai, Mária R, Zsolt Kohus, Szabolcs Káli, István Ulbert, Gábor Szabó, Zoltán Máté, Tamás F Freund, and Attila I Gulyás (2014). Physiological sharp wave-ripples and interictal events in vitro: what's the difference? *Brain* 137(Pt 2): 463–85.

Kerber, Karolin, Matthias Dümpelmann, Björn Schelter, Pierre Le Van, Rudolf Korinthenberg, Andreas Schulze-Bonhage, and Julia Jacobs (2014). Differentiation of specific ripple patterns helps to identify epileptogenic areas for surgical procedures. *Clinical Neurophysiology* 125(7): 1339–1345.

Klausberger, Thomas, Peter J Magill, László F Márton, J David B Roberts, Philip M Cobden, György Buzsáki, and Peter Somogyi (2003a). Brain-state and cell-type-specific firing of hippocampal interneurons in vivo. *Nature* 421(6925): 844–848.

Klausberger, Thomas, László F Márton, Agnes Baude, J David B Roberts, Peter J Magill, and Peter Somogyi (2003b). Spike timing of dendrite-targeting bistratified cells during hippocampal network oscillations in vivo. *Nature Neuroscience* 7(1): 41–47.

Kucewicz, Michal T, Jan Cimbalnik, Joseph Y Matsumoto, Benjamin H Brinkmann, Mark R Bower, Vincent Vasoli, Vlastimil Sulc, Fred Meyer, WR Marsh, SM Stead, et al. (2014). High frequency oscillations are associated with cognitive processing in human recognition memory. *Brain* 137(8): 2231–2244.

Latikka, Juha, Timo Kuurne, and Hannu Eskola (2001). Conductivity of living intracranial tissues. *Physics in Medicine and Biology* 46(6): 1611.

Le Van Quyen, Michel, Anatol Bragin, Richard Staba, Benoit Crépon, Charles L Wilson, and Jerome Engel (2008). Cell type-specific firing during ripple oscillations in the hippocampal formation of humans. *The Journal of Neuroscience* 28(24): 6104–10.

Malmivuo, Jaakko and Robert Plonsey (1995). *Bioelectromagnetism: principles and applications of bioelectric and biomagnetic fields.* Oxford University Press.

Menendez de la Prida, Liset and Andrew J Trevelyan (2011). Cellular mechanisms of high frequency oscillations in epilepsy: on the diverse sources of pathological activities. *Epilepsy Research* 97(3): 308–17.

Nunez, PL (1995). *Neocortical dynamics and human EEG rhythms.* Oxford University Press, Oxford.

Pangalos, Maria, José R Donoso, Jochen Winterer, Aleksandar R Zivkovic, Richard Kempter, Nikolaus Maier, and Dietmar Schmitz (2013). Recruitment of oriens-lacunosum-moleculare interneurons during hippocampal ripples. *Proceedings of the National Academy of Sciences* 110(11): 4398–4403.

Ray, Supratim, Nathan E Crone, Ernst Niebur, Piotr J Franaszczuk, and Steven S Hsiao (2008). Neural correlates of high-gamma oscillations (60-200 Hz) in macaque local field potentials and their potential implications in electrocorticography. *The Journal of Neuroscience* 28(45): 11526–36.

Roopun, Anita K, Jennifer D Simonotto, Michelle L Pierce, Alistair Jenkins, Claire Nicholson, Ian S Schofield, Roger G Whittaker, Marcus Kaiser, Miles A Whittington, Roger D Traub, et al. (2010). A nonsynaptic mechanism underlying interictal discharges in human epileptic neocortex. *Proceedings of the National Academy of Sciences* 107(1): 338–343.

Schevon, Catherine A, AJ Trevelyan, CE Schroeder, RR Goodman, G McKhann, and RG Emerson (2009). Spatial characterization of interictal high frequency oscillations in epileptic neocortex. *Brain* 132(11): 3047–3059.

Schmitz, Dietmar, Sebastian Schuchmann, Andre Fisahn, Andreas Draguhn, Eberhard H Buhl, Elisabeth Petrasch-Parwez, Rolf Dermietzel, Uwe Heinemann, and Roger D Traub (2001). Axo-axonal coupling: a novel mechanism for ultrafast neuronal communication. *Neuron* 31(5): 831–840.

Schomburg, Erik W, Costas A Anastassiou, György Buzsáki, and Christof Koch (2012). The spiking component of oscillatory extracellular potentials in the rat hippocampus. *The Journal of Neuroscience* 32(34): 11798–11811.

Simon, Anna, Roger D Traub, Nikita Vladimirov, Alistair Jenkins, Claire Nicholson, Roger G Whittaker, Ian Schofield, Gavin J Clowry, Mark O Cunningham, and Miles A Whittington (2014). Gap junction networks can generate both ripple-like and fast ripple-like oscillations. *European Journal of Neuroscience* 39(1): 46–60.

Spampanato, Jay and Istvan Mody (2007). Spike timing of lacunosom-moleculare targeting interneurons and CA3 pyramidal cells during high-frequency network oscillations in vitro. *Journal of Neurophysiology* 98(1): 96–104.

Staba, Richard J, Leonardo Frighetto, Eric J Behnke, Gary W Mathern, Tony Fields, Anatol Bragin, Jennifer Ogren, Itzhak Fried, Charles L Wilson, and Jerome Engel (2007). Increased fast ripple to ripple ratios correlate with reduced hippocampal volumes and neuron loss in temporal lobe epilepsy patients. *Epilepsia* 48(11): 2130–8.

Stacey, William C, Maciej T Lazarewicz, and Brian Litt (2009). Synaptic noise and physiological coupling generate high-frequency oscillations in a hippocampal computational model. *Journal of Neurophysiology* 102(4): 2342–2357.

Taxidis, Jiannis, Stephen Coombes, Robert Mason, and Markus R Owen (2012). Modeling sharp wave-ripple complexes through a ca3-ca1 network model with chemical synapses. *Hippocampus* 22(5): 995–1017.

Thomson, David J (1982). Spectrum estimation and harmonic analysis. *Proceedings of the IEEE* 70(9): 1055–1096.

Tort, Adriano BL, Horacio G Rotstein, Tamar Dugladze, Tengis Gloveli, and Nancy J Kopell (2007). On the formation of gamma-coherent cell assemblies by oriens lacunosum-moleculare interneurons in the hippocampus. *Proceedings of the National Academy of Sciences* 104(33): 13490–13495.

Traub, Roger D and Andrea Bibbig (2000). A model of high-frequency ripples in the hippocampus based on synaptic coupling plus axon–axon gap junctions between pyramidal neurons. *The Journal of Neuroscience* 20(6): 2086–2093.

Traub, Roger D, Diego Contreras, Mark O Cunningham, Hilary Murray, Fiona EN LeBeau, Anita Roopun, Andrea Bibbig, W Bryan Wilent, Michael J Higley, and Miles A Whittington (2005). Single-column thalamocortical network model exhibiting gamma oscillations, sleep spindles, and epileptogenic bursts. *Journal of Neurophysiology* 93(4): 2194–2232.

Traub, Roger D, John GR Jefferys, and Miles A Whittington (1997). Simulation of gamma rhythms in networks of interneurons and pyramidal cells. *Journal of computational neuroscience* 4(2): 141–150.

Urrestarazu, Elena, Rahul Chander, Francçois Dubeau, and Jean Gotman (2007). Interictal high-frequency oscillations (100–500 hz) in the intracerebral EEG of epileptic patients. *Brain* 130(9): 2354–2366.

Varga, Csaba, Peyman Golshani, and Ivan Soltesz (2012). Frequency-invariant temporal ordering of interneuronal discharges during hippocampal oscillations in awake mice. *Proceedings of the National Academy of Sciences* p. 201210929.

Wendling, Fabrice, Fabrice Bartolomei, Faten Mina, Clémént Huneau, and Pascal Benquet (2012). Interictal spikes, fast ripples and seizures in partial epilepsies–combining multi-level computational models with experimental data. *European Journal of Neuroscience* 36(2): 2164–2177.

Worrell, Greg A, Andrew B Gardner, S Matt Stead, Sanqing Hu, Steve Goerss, Gregory J Cascino, Fredric B Meyer, Richard Marsh, and Brian Litt (2008). High-frequency oscillations in human temporal lobe: simultaneous microwire and clinical macroelectrode recordings. *Brain* 131: 928–937.

Ylinen, a, a Bragin, Z Nádasdy, G Jandó, I Szabó, a Sik, and G Buzsáki (1995). Sharp wave-associated high-frequency oscillation (200 Hz) in the intact hippocampus: network and intracellular mechanisms. *The Journal of Neuroscience* 15(1 Pt 1): 30–46.

Figure Legends
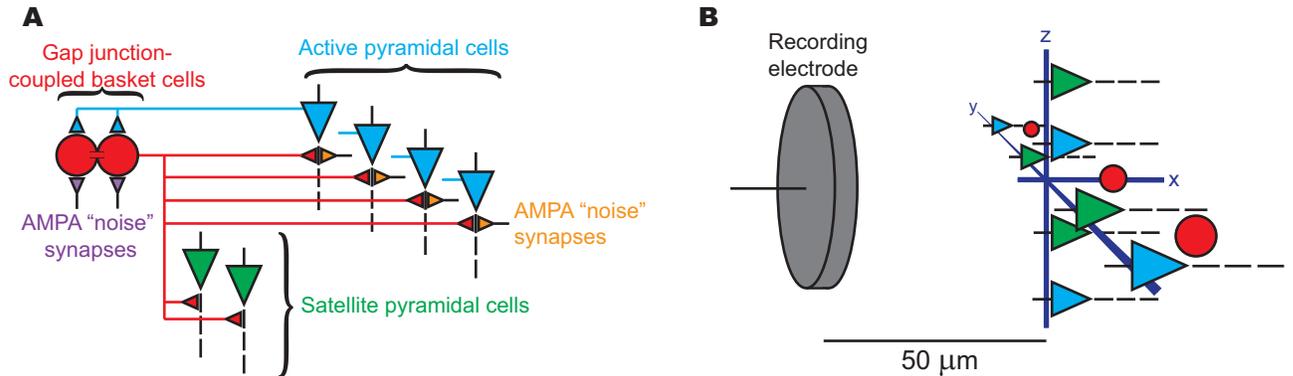
Figure 1. **Schematic of the computational model of hippocampus.** A: The model consisted of 80 active pyramidal cells, 3000 satellite pyramidal cells, and 20 basket cells. Active and satellite pyramidal cells were exactly the same except that active cells received noisy synaptic input which elicited firing, while satellite cells cells did not. Each basket cell was coupled with gap junctions to the nearest neighboring basket cells and sent GABAergic connections to all pyramidal cells (both active and satellite). Basket cells received feedback AMPAergic connections from active pyramidal cells, and they also received noisy synaptic input. All noisy input was independent from cell to cell throughout the network. B: All cells were distributed uniformly along two perpendicular axes in a plane 50 microns from the simulated recording electrode. The furthest cells were located 215 microns from the recording electrode.
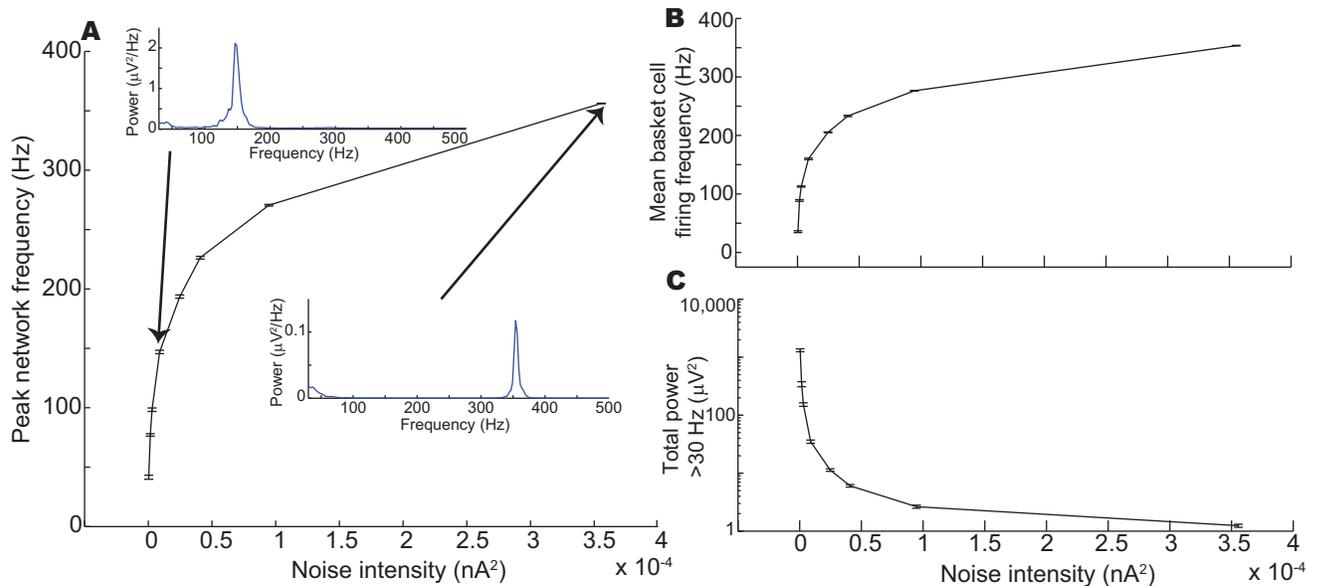
Figure 2. **HFOs resulting from noisy input to the basket cell population.** A: Peak network frequency (defined as peak frequency of the LFP power spectral density) increased as the intensity of noisy synaptic input to basket cells increased. The insets depict two example PSD functions. Note the difference in scale between the vertical axes of the two insets, indicating the extreme diminution of oscillation amplitude as frequency increased. Individual PSDs were obtained from 1000 ms of simulation data. B: Mean basket cell firing frequency very closely tracked peak network frequency for a given level of synaptic input. C: Total LFP power above 30 Hz decreased dramatically as noisy intensity (and peak network frequency) increased. Therefore while it was possible for noisy input to basket cells to elicit rhythms with fast ripple frequencies, such rhythms exhibited very low amplitude.
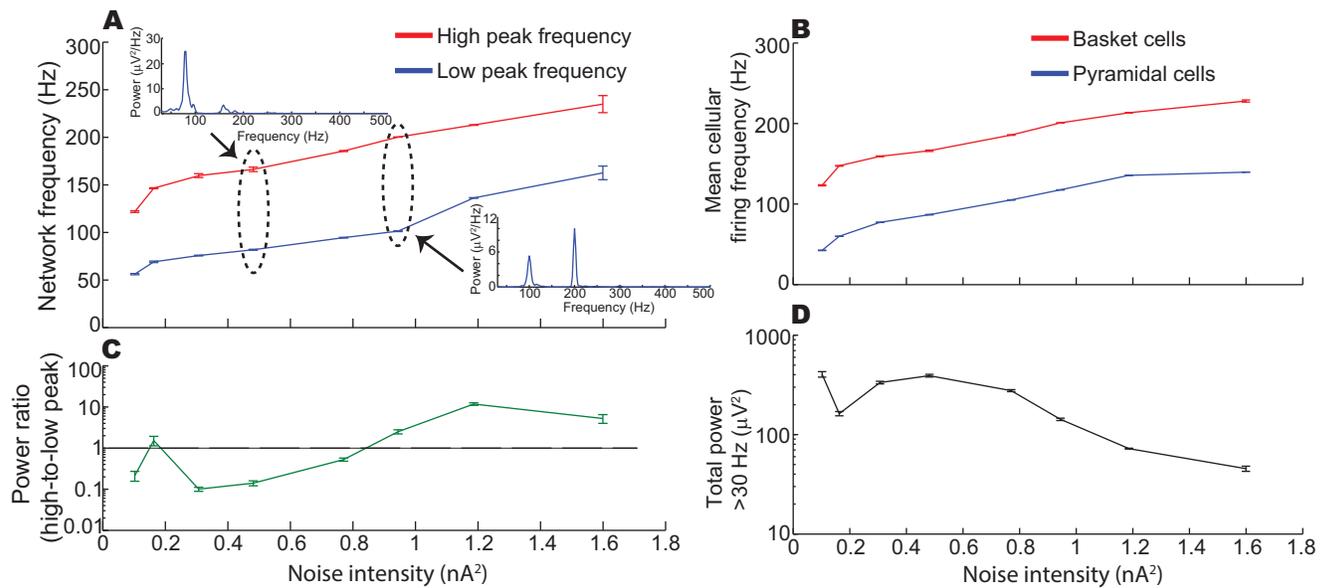
Figure 3. HFOs resulting from noisy input to the active pyramidal cell population. A: Increased noise intensity to pyramidal cells stimulated increases in the two highest-power frequencies observed in the LFP PSDs, which were generally bimodal (see insets). Note that the network was incapable of generating rhythms faster than 250 Hz, in contrast to simulations in which basket cells received direct input (Fig. 2A). B: High-frequency and low-frequency spectral bumps corresponded to the mean firing rates of basket cells and active pyramidal cells, respectively. C: Relative dominance between the two spectral bumps varied with noise intensity, as shown in this plot of the ratio of the maximum power of the high-frequency peak to the maximum power of the low-frequency peak. Ratios greater than 1 (demarcated by the dashed line) imply that the high-frequency peak dominated the low-frequency peak. D: Total LFP power above 30 Hz tended to decrease somewhat with increasing noise intensity, though not nearly as dramatically as when basket cells received noisy input (Fig. 2D).
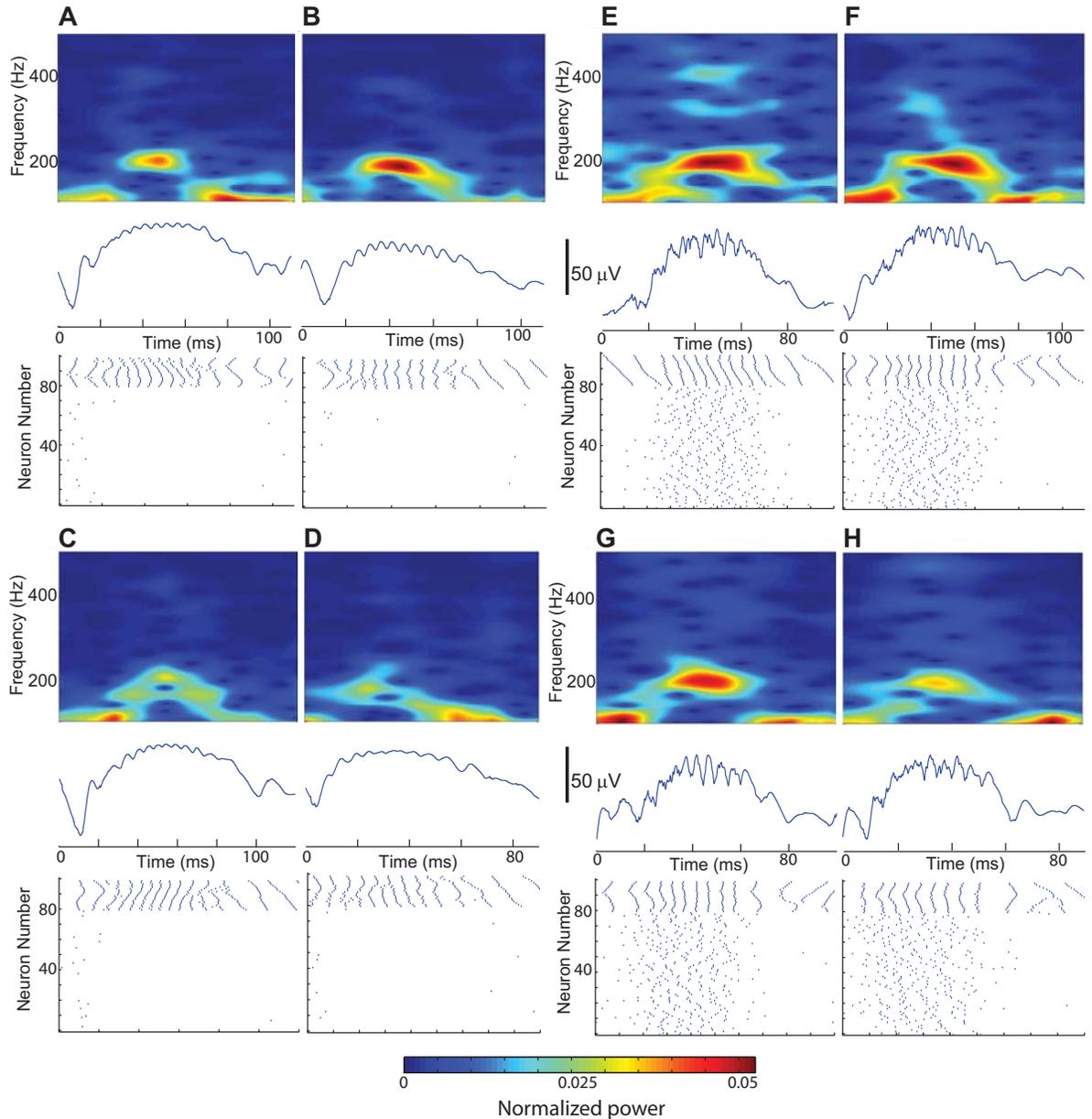
Figure 4. Ripple generation by noisy stimulation of either basket cells or pyramidal cells. A-D: Examples of sharp-wave ripples induced by activation of the basket cell population (ID numbers 81–100 in the raster plot). Note the extreme sparsity of spiking of pyramidal cells (ID numbers 1–80 in the raster plot). LFP ripple oscillations were produced by IPSPs in all 3080 pyramidal cells. (The 3000 satellite cells never fired action potentials and are not included in the raster plots.) E-H: Examples of sharp-wave ripples induced by activation of the active pyramidal cell population. The increased pyramidal cell spiking induced increased basket cell activity. Their inhibitory influence restricted the dominant frequency component to ≈200 Hz.
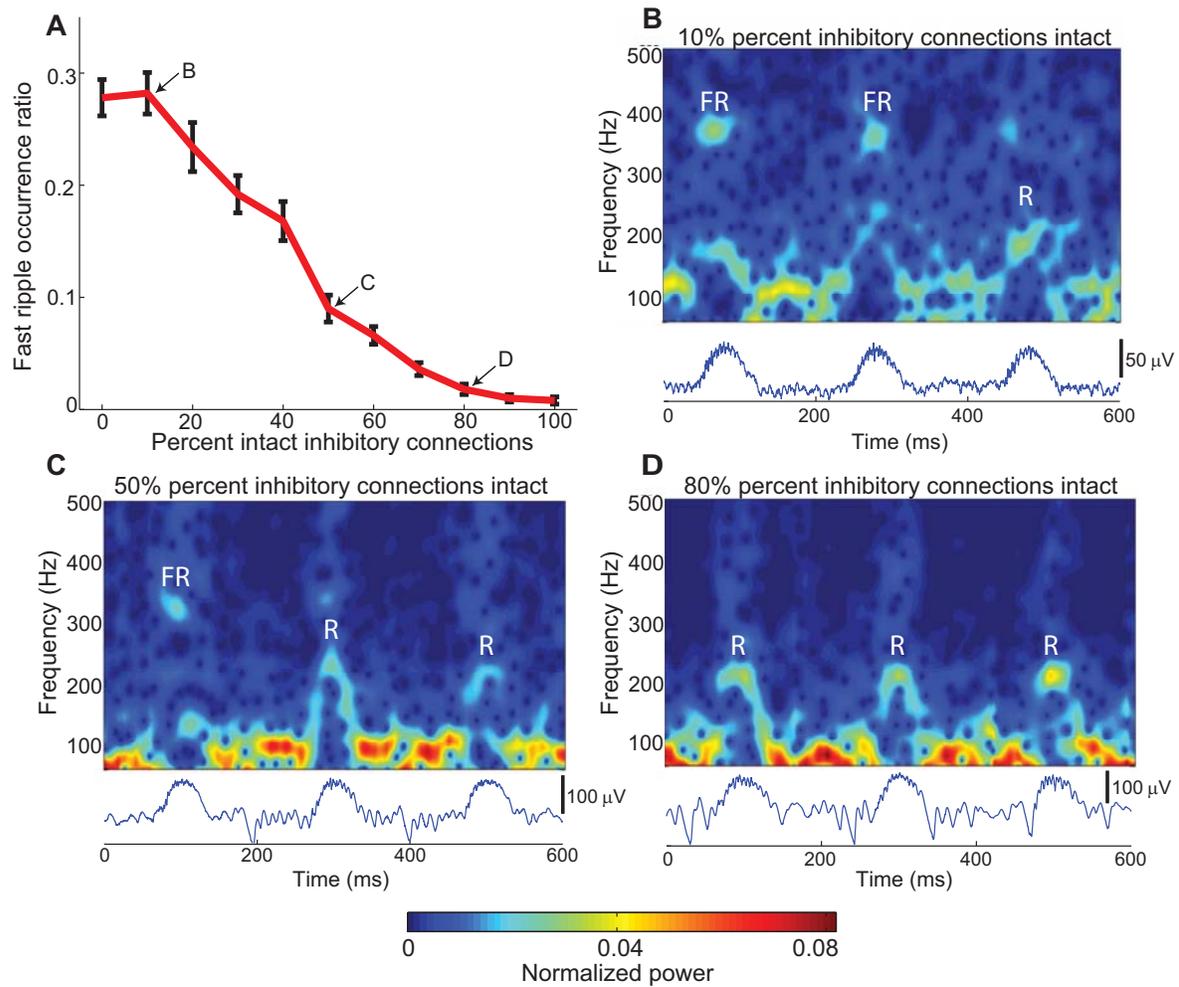
Figure 5. Effect of diminished inhibition on fast ripple incidence. Simulations were conducted in which 50 separate sharp waves were induced by increasing noisy input to active pyramidal cells. The percentage of intact inhibitory connections from basket cells to both active and satellite pyramidal cells was modulated. A fast ripple was defined to occur when the peak energy in the fast ripple band (>250 Hz) exceeded the peak energy in the ripple band (100–250 Hz). A: Proportion of sharp waves which exhibited fast ripples, as a function of intact inhibitory connections. As inhibitory connections diminished, fast ripple incidence increased dramatically. (Error bars represent s.e.m. over ten simulations, each with 50 induced sharp waves.) B–D: Example LFP's and spectrograms for three levels of intact inhibition, each with three example sharp waves. FR=fast ripple episode, R=ripple episode.
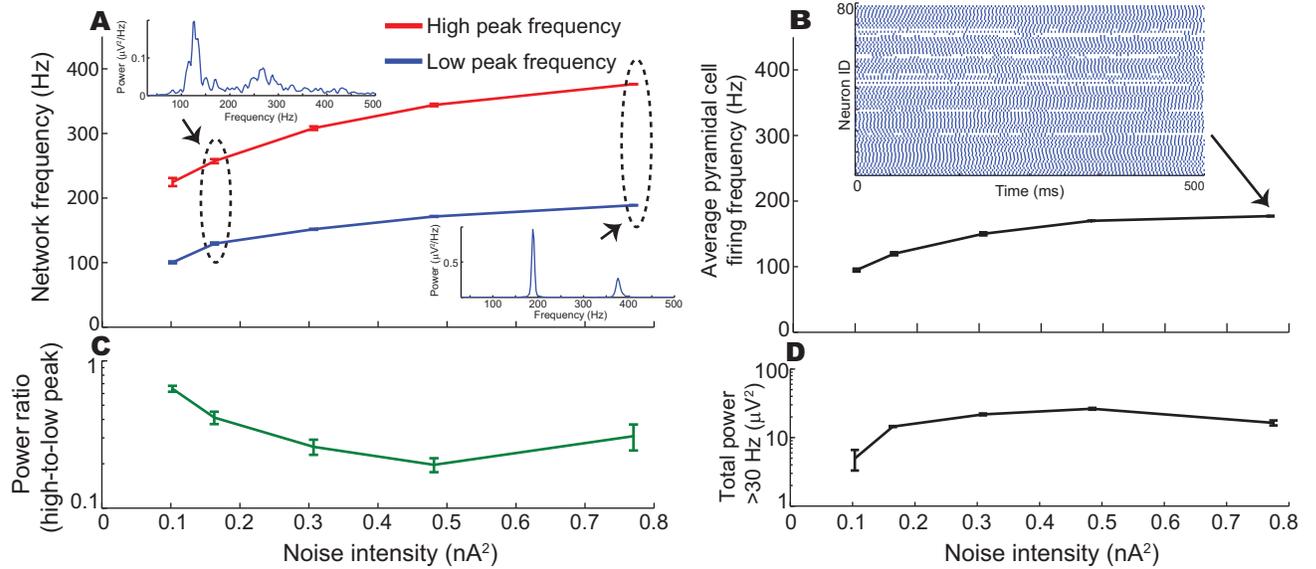
Figure 6. HFOs resulting from noisy input to 80 uncoupled pyramidal cells. A: Two highest-power frequecy peaks in the PSD as a function of noise intensity. PSDs were generally bimodal, and grew more coherent as noise intensity increased. Note how the high-frequency peaks reached fast ripple frequencies and represent a harmonic of the low-frequency peaks. B: The low-frequency peak in the PSDs from panel A corresponded to the average cellular firing frequency. Inset shows a raster plot of network activity resulting from the highest noise intensity that still sustained network oscillations. Noticeable horizontal gaps in the raster plot indicate neurons going into momentary depolarization block. Higher noise intensity resulted in virtually the entire network going into depolarization block. C: Ratio of peak power of the high-frequency peak to peak power of the lower-frequency peak. D: Total LFP power above 30 Hz as a function of noise intensity. As in Fig. 3, there were coherent oscillations even at high noise intensities.
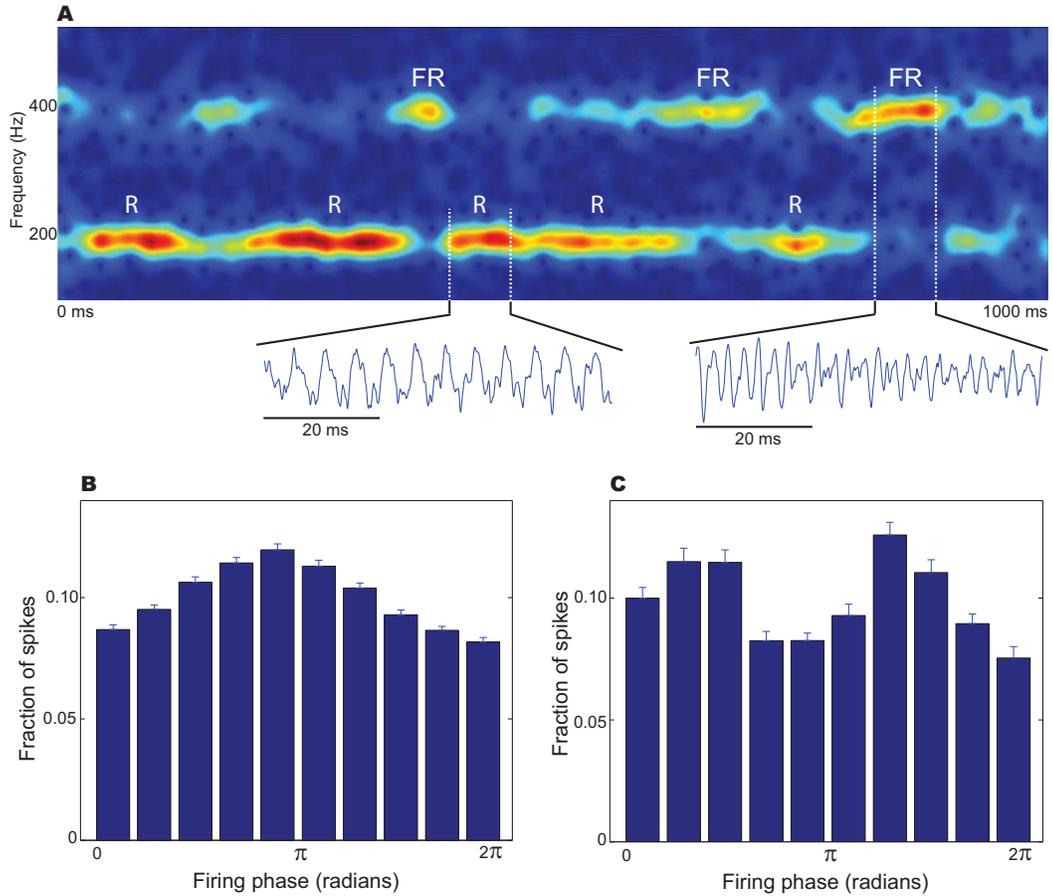
Figure 7. Emergence of fast ripples in an uncoupled, asynchronously-spiking network. Using the same parameters as the highest-frequency data in Fig. 6, a 20,000 ms simulation was performed to identify the emergence of HFOs in a network of 80 uncoupled pyramidal cells driven by high levels of uncorrelated noisy input. A: LFP spectrogram of a 1000-ms interval demonstrates that both ripple (R) and fast ripple (FR) episodes emerged sporadically. B: Spike-timing histogram relative to ripple phase, averaged over all 78 observed *ripple* episodes. C: Spike-timing histogram relative to ripple phase, averaged over all 26 observed *fast ripple* episodes. Ripples occurred when the 80 cells achieved brief unimodal spike time distibution, and fast ripples occurred when the distribution was transiently bimodal.
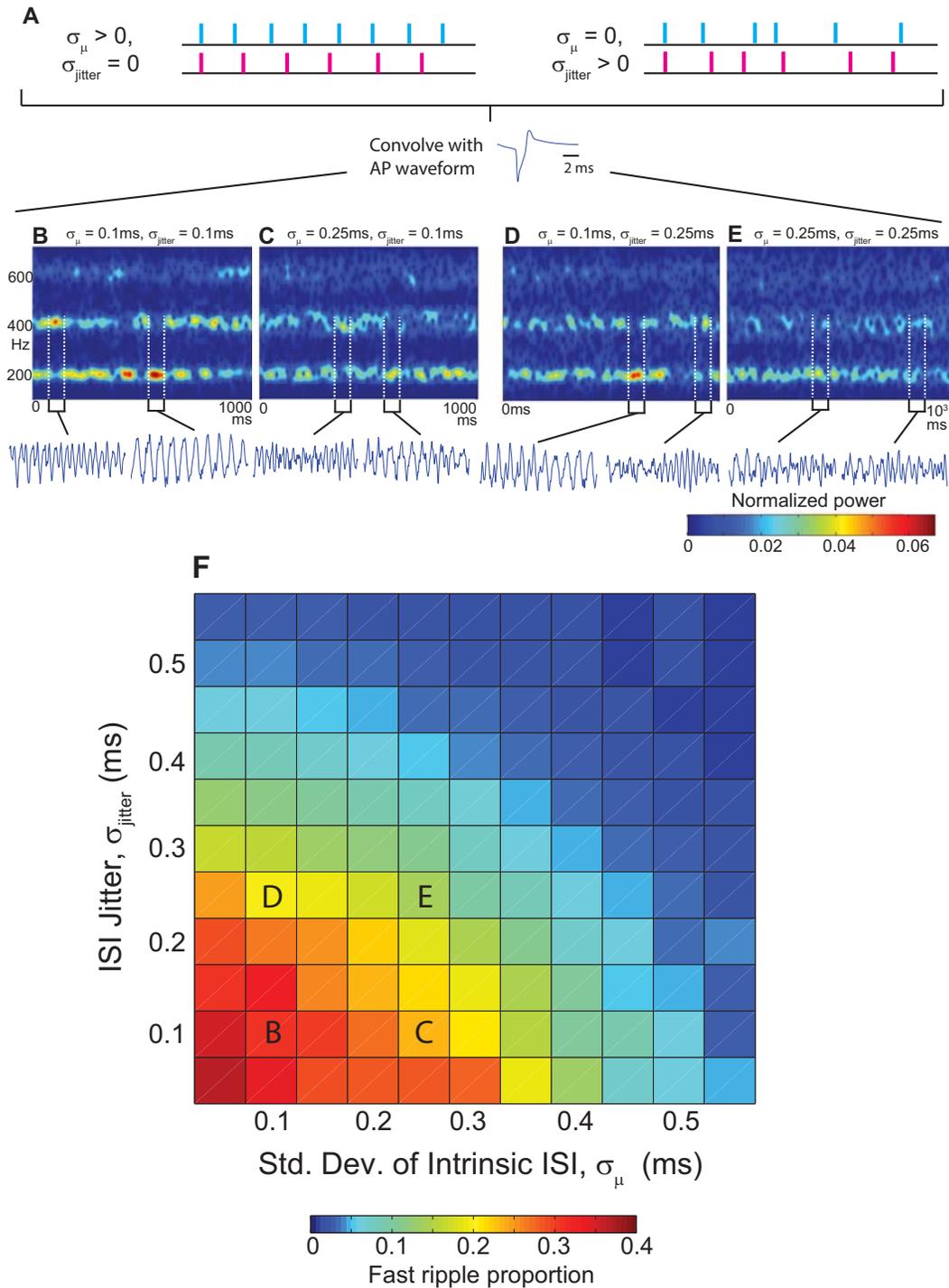
Figure 8. Fast ripple occurrence ratio for constructed LFP's generated from AP waveforms. A: Constructed LFPs were produced by first generating trains of event times which had two sources of variation: (1) different trains had different values for their intrinsic firing rates, with greater values of σ_μ implying greater firing rate heterogeneity between different cells, and (2) within each train there was "jitter" in the inter-spike interval (ISI). These spike trains were then convolved with AP waveforms and summed to yield the constructed LFP. Red and blue spike trains show examples of firing times of two different "cells" with different firing rates (left) or different ISI jitter (right). B–E: Spectrograms and LFP samples from the constructed LFPs generated using the indicated parameters. Fast ripples frequently emerged from random network firing. F: Fast ripple proportion as a function of the two sources of heterogeneity in the model. Fast ripple proportion was simply the proportion of total time that the peak frequency in the 100-700 Hz band was greater than 250 Hz..
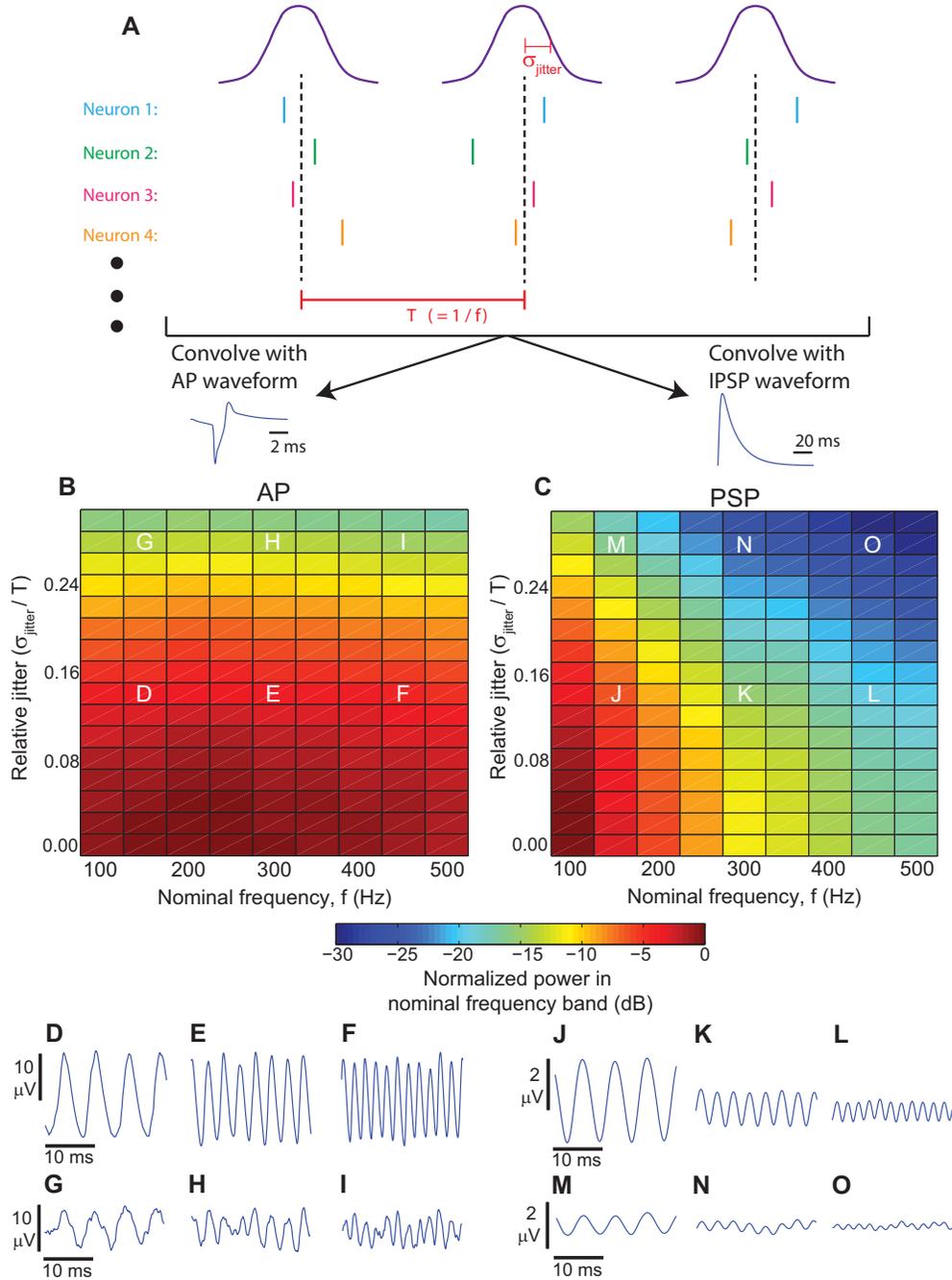
Figure 9. Capability of AP versus PSP events to produce HFOs of varying frequency. A: Constructed LFPs were produced by generating synchronous network bursts of either AP or PSP events at periodic intervals, with nominal frequency f and random variation defined by σ_{jitter}. B,C: Color encodes the power within the frequency band $f \pm 5$ Hz, normalized by the maximum power observed across all parameters in each waveform. For both APs and PSPs, increased jitter caused the LFP output to become less coherent and the normalized power to drop. On the other hand, increasing frequency of network bursts had little effect on AP-dominated oscillations, but resulted in significant attenuation of PSP-dominated oscillations. D–I: Representative AP-dominated LFPs associated with the corresponding combinations of parameters indicated in panel B. Note how amplitude is unchanged as oscillation frequency increases. J–O: Representative PSP-dominated LFPs associated with the corresponding combinations of parameters indicated in panel C. Note the difference in scale bars, and how amplitude is dramatically attenuated as oscillation frequency increases. Thus, APs can robustly produce the full range of HFOs, whereas PSPs are unlikely to produce HFOs over 200 Hz.
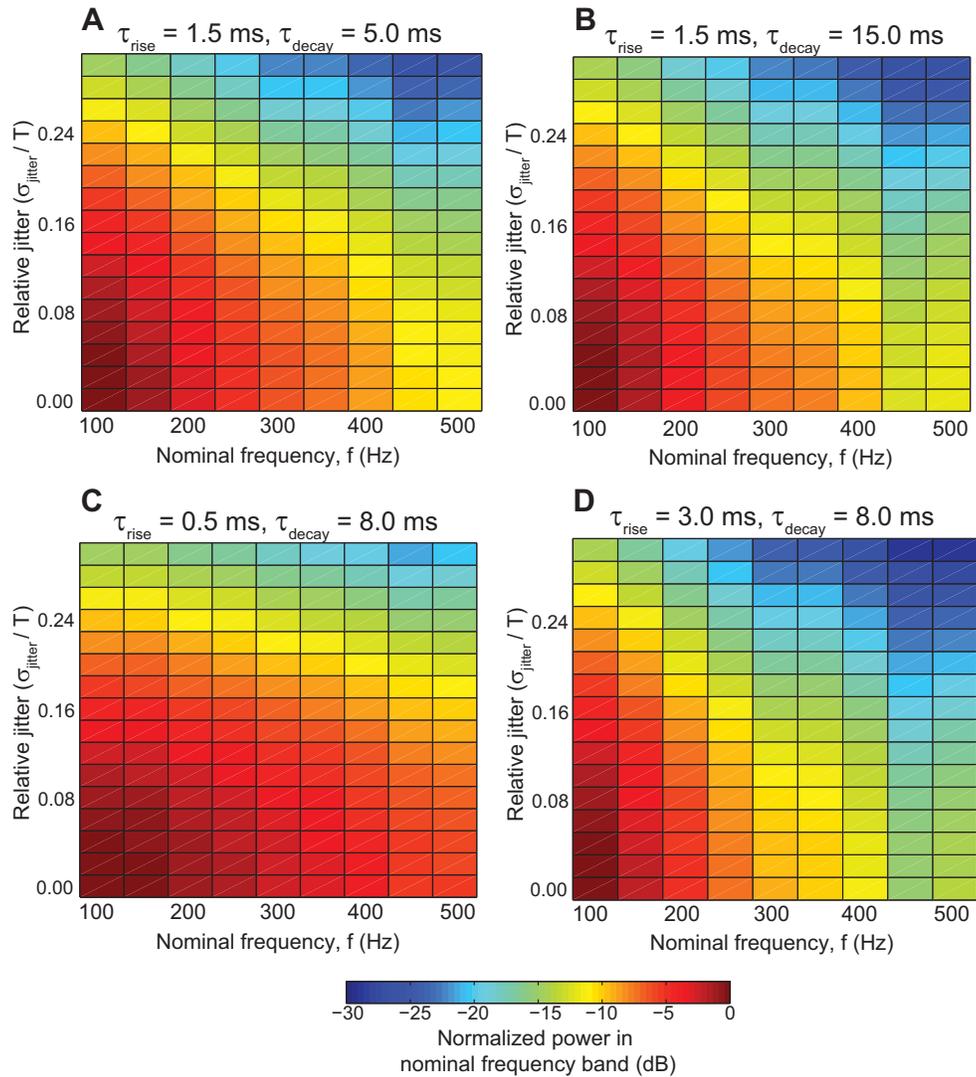
Figure 10. Effects of synaptic parameters on HFOs. LFPs were constructed as in Fig. 9C, except that GABAergic synaptic rise and decay times were modified from their standard values ($\tau_{\mathrm{rise}} = 1.5$ ms and $\tau_{\mathrm{decay}} = 8.0$ ms). A-B: Changing τ_{decay} had little effect on the HFO output. C-D: Very fast τ_{rise} time (0.5 ms) enabled IPSPs to produce HFOs more robustly.